Article

Using a Fragment-Based Approach to Identify Alternative Chemical Scaffolds Targeting Dihydrofolate Reductase from *Mycobacterium tuberculosis*

João A. Ribeiro, Alexander Hammer, Gerardo A. Libreros-Zúñiga, Sair M. Chavez-Pacheco, Petros Tyrakis, Gabriel S. de Oliveira, Timothy Kirkman, Jamal El Bakali, Silvana A. Rocco, Mauricio L. Sforça, Roberto Parise-Filho, Anthony G. Coyne, Tom L. Blundell, Chris Abell, and Marcio V. B. Dias*

Read Online

| ACCESS | Metrics & More | Article Recommendations | SI Supporting Information |

ABSTRACT: Dihydrofolate reductase (DHFR), a key enzyme involved in folate metabolism, is a widely explored target in the treatment of cancer, immune diseases, bacteria, and protozoa infections. Although several antifolates have proved successful in the treatment of infectious diseases, they have been underexplored to combat tuberculosis, despite the essentiality of *M. tuberculosis* DHFR (MtDHFR). Herein, we describe an integrated fragment-based drug discovery approach to target MtDHFR that has identified hits with scaffolds not yet explored in any previous drug design campaign for this enzyme. The application of a SAR by catalog strategy of an in house library for one of the identified fragments has led to a series of molecules that bind to MtDHFR with low micromolar affinities. Crystal structures of MtDHFR in complex with compounds of this series demonstrated a novel binding mode that considerably differs from other DHFR antifolates, thus opening perspectives for the development of relevant MtDHFR inhibitors.

KEYWORDS: fragment-based drug discovery, Mycobacterium tuberculosis, dihydrofolate reductase
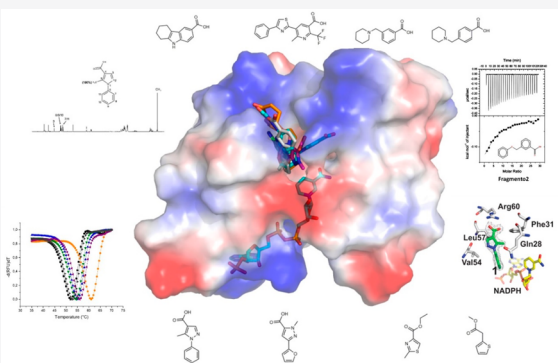
DHFR is a key enzyme involved in the biosynthesis of tetrahydrofolate, an essential cofactor for the biosynthesis of purine and thymidine nucleotides and several amino acids.[1] DHFR is a well-established target for human diseases, including cancer[2] and autoimmune diseases,[3] as well as for infectious diseases.[4−6] However, drugs such as antifolates used for human and infectious disease treatment differ considerably, due to differences in binding sites of microorganisms and human DHFRs.

Despite the importance of DHFR inhibitors for human health, no drug was specifically designed to target MtDHFR, or has shown sufficient efficacy against whole cells. There is an extensive scientific literature describing different strategies aiming to identify or synthesize inhibitors against MtDHFR with antituberculosis clinical applications,[7−9] including compounds with dual inhibitory activity against MtDHFR and the MtDHFR-like enzyme Rv2671.[10] Also, *p*-aminosalicylic acid, a second-line drug used in the tuberculosis treatment, was proposed to be an alternative substrate of the folate pathway, and the product of the metabolism has been shown to inhibit MtDHFR and the FAD-dependent thymidylate synthase.[10−13]

Tuberculosis is a major infectious disease and causes more deaths than any other bacterial species.[14] Various efforts have

been focused on new strategies to combat tuberculosis, but only recently two new drugs with novel action mechanisms have been approved for use.[15] The discovery of new drugs against tuberculosis is particularly demanding because of the long regime therapy and the emergence of resistant strains against all used drugs. In this context, the development of new strategies to fight tuberculosis is urgently needed.

Fragment-based drug discovery (FBDD) is a successful approach that was introduced in several pharmaceutical companies, and over 40 new drugs derived from fragments have been entered into clinical trials, in which four of them were approved in the past 20 years.[16] The FBDD approach involves the identification of low molecular weight compounds that bind to a specific protein target through a range of biophysical methods[17,18] and the validated molecules are
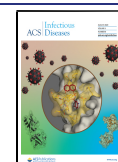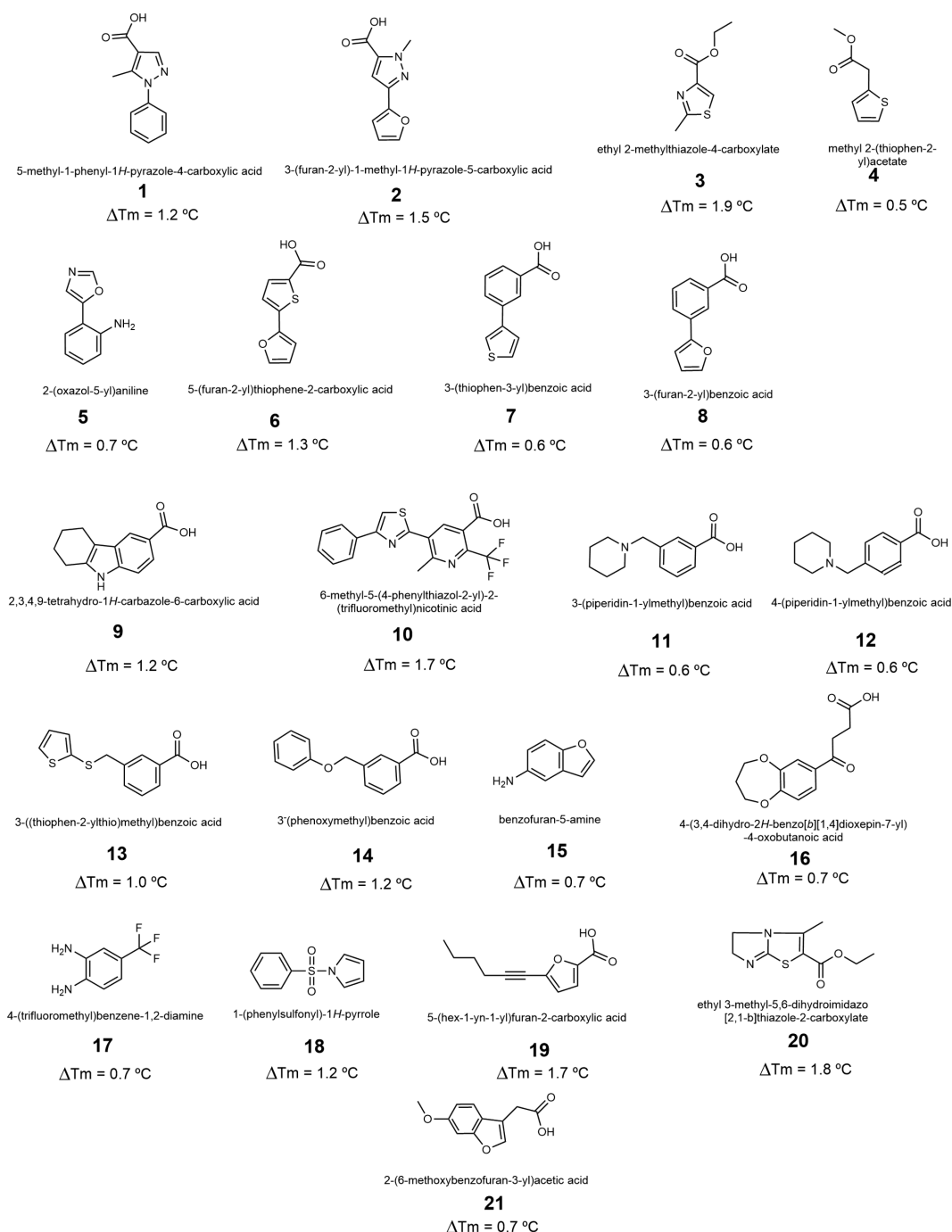
Figure 1. Fragments validated by STD-NMR. The ΔT_m is included below each structure.

considered an attractive starting point for the synthesis of high-affinity compounds.[19] Although FBDD has been applied to several targets from *M. tuberculosis*[20−22] and new compounds have been identified to inhibit the growth of this bacterium,[21,23] this technique has not been applied to MtDHFR or any other chromosomal DHFR.

In this work, an FBDD approach was successfully applied using a range of biophysical techniques to identify compounds that have completely novel scaffolds that bind to the MtDHFR active site, and one of them was used as a starting point for further elaboration. This fragment was the base for further screening using an in house library leading to the identification of compounds with low micromolar affinity.

RESULTS AND DISCUSSION

Screening by DSF and Validation by 1D STD-NMR. MtDHFR-NADPH was screened against 1250 compounds selected following the rule of three.[24] Trimethoprim, which gave a ΔT_m of +10 °C (Figure S1), was used as a positive control. Positive hits were defined as fragments that gave a ΔT_m of ≥0.5 °C above 53.4 °C. About 37 statistically positive hits (Figure S2) represent about 2.8% of the library with significant chemical diversity.

A large number of identified compounds shared similar features, including a carboxylic acid at the *meta* position of a benzene ring, which is generally linked by a single bond to another comprising two heterocyclic rings (Figure 1).

Interestingly, it has been reported that compounds with stilbenoid, deoxybenzoin, and chalcone moieties, which have similar scaffolds to some of our compounds, also showed affinity to *E. coli* DHFR and had an uncompetitive mechanism of inhibition[25] (Figure S2).

From 37 molecules that stabilized MtDHFR above 0.5 °C in the DSF assay, we rescreened 30 fragments (Figure S2) using 1D STD-NMR and confirmed 21 fragments molecules (Figure S3) that interact with the protein, which represents about 70% of the molecules (Figure 1).
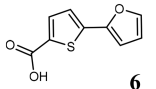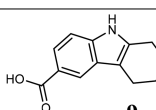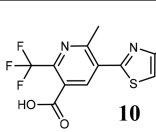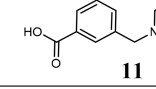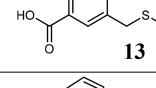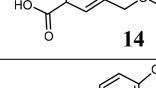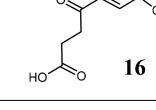
Although 1D STD-NMR is routinely used to rescreen the hits identified by DSF, we used this technique to identify epitopes from the fragments that are essential for the interaction with the target.[26,27] The protein−fragment interactions were confirmed by proton signals in the difference spectra (on-resonance−off-resonance). The data of difference were normalized and the signal/noise rate was calculated with a threshold of ≥5 for this relation. For normalization, we have attributed to the protons with the most intense STD signal as 100%, and they have been used as reference for the calculation of the intensity percentage for the other additional protons of the ligand. Proton signals were satisfactorily confirmed for 21 fragments and the corresponding protons attributed in the spectra are identified by numbers in the structures (Figure S3). Interestingly, the 1D STD-NMR signals show that the benzoic acid for most of the fragments should have close contacts with the protein as the STD enhancement for this group is nearly 100%. This region should bind tightly to the target and have a key role in the interaction. Also, it is observed that most of the compounds that have this benzoic acid moiety are linked to other heterocycles, as thiophene (**7** and **13**), furan (**8**), carbazole (**9**), and nonaromatic heterocycles, such as piperidine (**11** and **12**). The fragments **11** and **12** are similar molecules and they differ only in the position of the carboxylic acid at the benzene ring, which for **11** is at *meta* position and in **12** is *para*. As observed for most of the fragments with benzoic acid, **11** has an intense signal of protons, and consequently, the *meta* configuration of the carboxylic acid attached to the benzene ring could be a key factor for the strong interaction. The crucial role of the benzoic acid for the interaction suggested that this group could perform an ionic interaction with one of the arginines within the MtDHFR active site, such as Arg60, mimicking the interaction of glutamate moieties of dihydrofolate. The *meta* position of the carboxylic acid could contribute to orientate this group toward the positive charges of the active-site cavity. The importance of the carboxylic acid attached to a ring could also be observed for compounds **1**, **2**, **6**, **10**, and **19**, where these, instead of having benzene ring, have the carboxylic acid attached to a heterocycle such as a pyrazole, thiophene, and furan so that a maximum resonance could be observed for carbons of the ring. The 1D STD-NMR spectra also suggest the importance of different rings linked since the transference of resonance is highly significant. Moreover, there is a clear preference of aromatic rings, including both benzene or heterocycles, including pyrazole (**1**), thiazole (**3**), oxazole (**5**), and pyrrole (**18**). Interestingly, compound **16**, which has the benzoic acid fused with a dioxepine, but the carboxylic acid attached to the benzene ring through a 4-oxo-butyl linker, could have a key role in the interaction with the protein.

Several other fragments were confirmed to interact with MtDHFR. Another group of fragments comprises of small compounds with neither linked rings nor carboxylic acid (**3**, **4**,

15, **17**, and **20**). Although two fragments (**5** and **18**) have linked rings, they do not have carboxylic acid groups and three of the fragments have an ester group instead (**3**, **4**, and **20**). Although **21** also has a carboxylic acid, it is attached to a benzofuran ring and probably it should bind distinctly to the other *meta*-carboxylic acid-containing fragments.

Calorimetric Analysis of Fragments Selected as Hits for DHFR. The 21 fragments confirmed to bind to MtDHFR through DSF and 1D STD-NMR were further characterized by ITC (Table S1 and Figure S4). Table 1 shows the affinity and

**Table 1. Calorimetric Analysis of Fragments against MtDHFR**
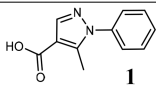
Fragment	ΔT$_m$ (°C)	Kd (mM)	LE
1	1.2	0.64±0.12	0.28
6	0.7	2.5±0.2	0.25
9	1.2	0.098±0.02	0.34
10	1.7	0.095±0.005	0.23
11	0.6	3.2±0.4	0.21
13	1.0	0.75±0.09	0.26
14	1.2	0.50±0.02	0.26
16	0.7	2.7±0.4	0.19

LE for the 8 best fragments. Except for the titration with **1**, all thermograms were fitted using a unique site model, indicating that the MtDHFR active site is occupied only by one ligand molecule (Figure S4). Interestingly, the thermogram curve for **1** indicated a sequential site model, suggesting that this molecule might bind in two distinct regions of the active site. **9** and **10** were the fragments that have the highest affinity among the tested molecules, with 95 and 98 *μ*M, respectively, although **9** also has the highest LE, 0.34.

Structural Basis of the Interaction of MtDHFR with Selected Fragments. A total of 9 crystal structures were obtained with a resolution ranging from 2.5 to 1.7 Å for MtDHFR in complex with different fragments (Table S2). Although the binding affinity for fragments **3** and **16** was not measured, their interaction modes with MtDHFR, despite the

low occupancy of these molecules, were obtained. Table S2 shows the data processing, refinement, and quality of the stereochemistry of the MtDHFR structures in complex with fragments. All structures have the NADPH engaged in the active site as described previously,[28,29] and the protein did not undergo significant conformational changes in the presence of fragments (Figure S5).

To facilitate the description of fragment interaction with the protein, we distinguished four different subregions of the active site groove of MtDHFR:NADPH (Figure 2): (1) active site
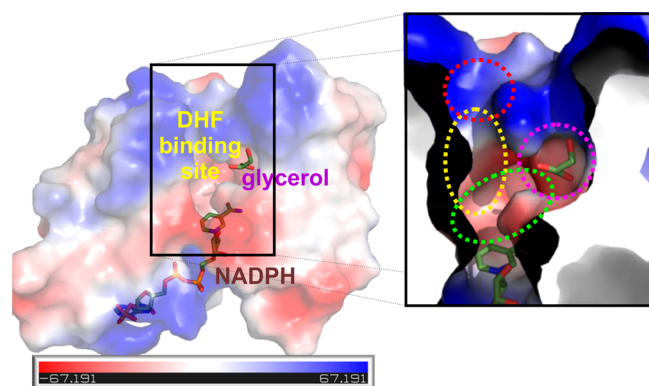
Figure 2. MtDHFR active site groove and subregions. The figure shows the DHF and glycerol binding cavities. In the inset, we have specified 4 subregions of the active site. (1) (in red) A positively charged region that binds the glutamate moiety of DHF; (2) (in yellow) the central region, where the PABA moiety sits, that is apolar; (3) (in green) where the positive dipyrimidine ring of DHF stacking with nicotinamide moiety of NADPH; and (4) (in magenta) the glycerol-binding site, an exclusive pocket of MtDHFR in comparison to hDHFR.

entrance, with a positive charge, (2) central region of the active site or PABA binding site, a slightly apolar region, (3) dipyrimidine binding site, with strong negative charges, and (4) the glycerol-binding site, a specific region found in MtDHFR, not observed in human DHFR (hDHFR).[29]

All the structures of MtDHFR:NADPH in complex with fragments show electron density for fragments in three regions of MtDHFR:NADPH, which includes the entrance (1), PABA binding site (2), and glycerol binding site (4); surprisingly, we did not observe any fragment completely occupying the dipyrimidine binding site (3), which is one of the most explored regions of DHFR in the development of new inhibitors. Most of the compounds that have the carboxylic acid linked to a phenyl or a heterocyclic ring indicate strong interaction with the active site entrance (region 1), where the carboxylic acid is interacting through ionic interaction with Arg60. The interactions of the compounds in that region explain and confirm our results from 1D STD-NMR, which indicate a 100% proton transference of this region and the high enthalpic contribution for the binding, characterizing a strong polar interaction. The importance of a second ring (phenyl or heterocyclic) could also be confirmed since in most cases these rings exhibit π-interactions with Phe31 on the PABA binding site (subregion 2), as well as interactions with other residues, such as Leu50 and Ile94 (Figure 3). These interactions also confirm the results of ITC indicating high entropic contributions for the interaction of fragments (Table S1). In addition, because of the proximity of the second ring of these

compounds with the NADPH nicotinamide group, we can also observe an edge−π interaction with this group and then slightly reaching the subregion 3.

Fragment **2** was unique in that it did not interact with Arg60 but rather is hydrogen-bonded to the side chain of Gln28 even having the carboxylic acid in *meta* position while maintaining the interaction with Phe31 through its furan group as do the other fragments from this group. Interestingly, fragment **1** was unique in occupying the glycerol-binding site (4), while its carboxylic acid makes a hydrogen bond with the side chain of Gln28. Since the glycerol-binding site is a feature observed in MtDHFR in contrast to hDHFR, this fragment could be an excellent starting point to obtain specific drug leads against tuberculosis. As expected, an electron density for fragment **1** was also observed in the PABA-binding site (2) and interacting with Arg60 in the active site entrance (1), also supporting the results of ITC that indicated that this molecule has a sequential binding mode. However, as the average B-factor for this second molecule is higher than the first one, probably the binding on the glycerol-binding site just occurs after the complete occupation of the PABA-binding site.

Although there is a structural similarity of **6**−**8** to **1** and **2**, we were not able to obtain the structures of these fragments even though they have a carboxylic acid group. As the affinities of **2**, **5**−**8** are low, we suggest that a higher affinity interaction of this fragment scaffold would be necessary for the association of "*meta*-position" in a five-membered ring with a phenyl ring, a characteristic observed only for **1**. Interestingly **1** and **2** are also very similar compounds, but the binding modes of these two molecules are quite different, indicating that the phenyl and furan groups, as well as the position of the methyl group attached to the pyrazole ring, might have a strong influence on the orientation of these compounds in the enzyme active site.

Fragments **3** and **17** were the only ligands in the series that do not have a carboxylic acid for which we were able to obtain the crystal structures; however, we could observe the binding mode in only one protomer of the asymmetric unit for both compounds and we were not able to obtain the affinity of these compounds by ITC. These two molecules have distinct structures since **3** is a thiazole ethyl ester and **17** is a trifluoromethylphenyl diamine. Interestingly, both molecules bind in the PABA binding site (3), despite their different orientations, and make only nonpolar contacts with the active site residues.

Fragment **10** is the largest for which we have obtained the crystal structure complex with MtDHFR:NADPH. Although its thiazole ring is binding in the same position of the PABA moiety of MTX, the phenyl ring reaches a deeper point in the active site of MtDHFR and sits close to the pyrimidine moiety of MTX stabilizing several nonpolar contacts with this active site region (Figure S6).

The chemical structures of the fragments **13** and **14** are similar and they differ in a second ring in which **13** and **14** have a thiophenyl-thiomethyl and a phenoxymethyl and they bind in the similar position at the MtDHFR active site (although the twist caused by the sulfur atom in contrast to the oxygen in the linker between the two rings). The similar pose of these fragments in the MtDHFR active site was expected since their affinities (K_D) were similar, 0.752 and 0.502 mM for **13** and **14**, respectively. Interestingly, although these compounds are smaller than **10**, the thiophene and the phenyl ring sit in the same position of the compound **10** phenyl ring,
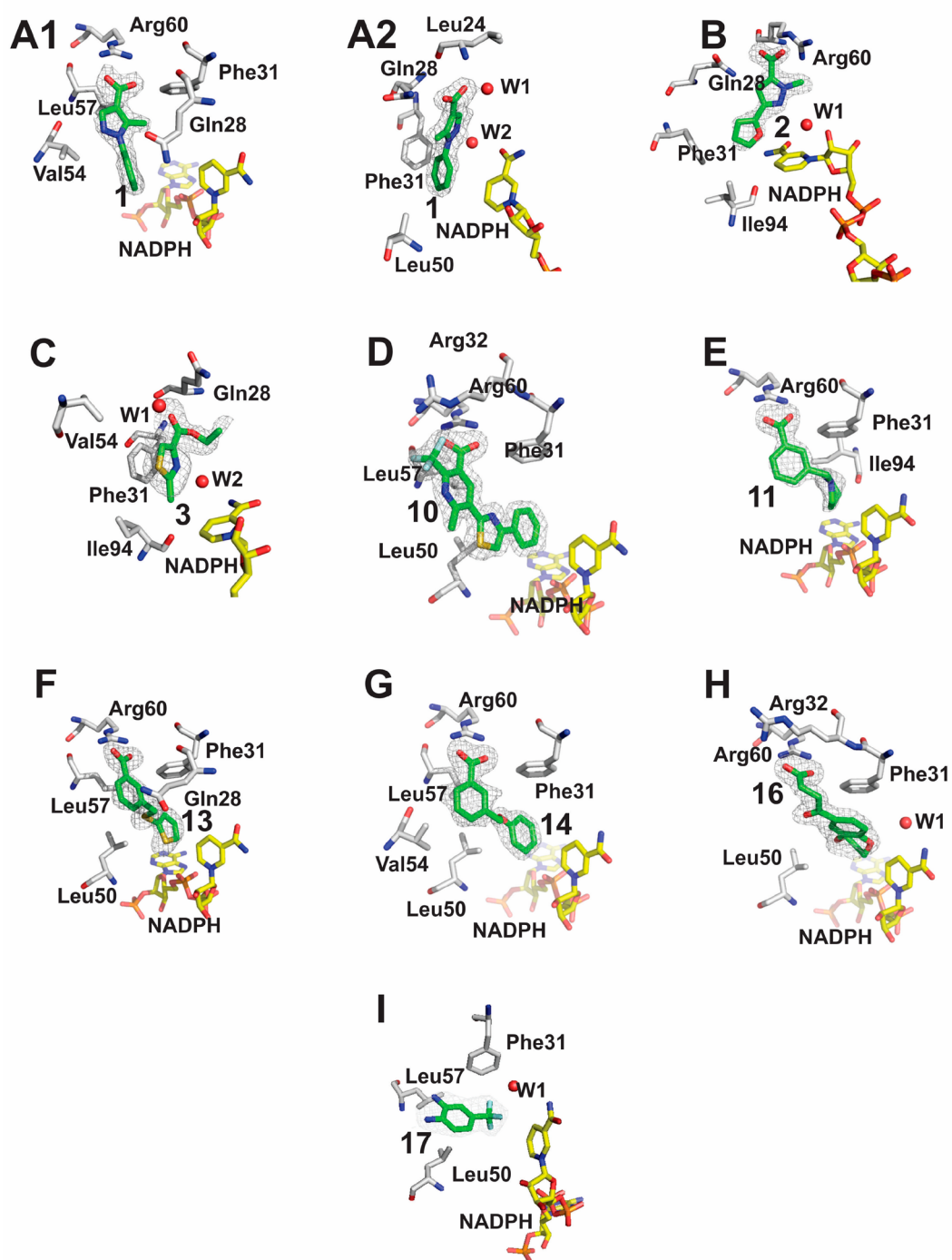
Figure 3. Crystal structures and binding modes of fragments that interact with MtDHFR:NADPH. (A) **1**. Fragment **1** binds in two different pockets of MtDHFR (**A1** and **A2**); (B) Fragment **2**; (C) Fragment **3**; (D) Fragment **10**; (E) Fragment **11**; (F) Fragment **13**; (G) Fragment **14**; (H) Fragment **16**; (I) Fragment **17**. The electron density contours are from a $2F_o-F_c$ map with 1σ. W1 are water molecules.

and the linker between the two rings adopts the position of the PABA moiety of MTX (figure not shown).

The role of the carboxylic acid in the *meta* position could be further validated in the structure of MtDHFR:NADPH in complex with **11**. Even though we performed several attempts to obtain the structure for the complex with **12**, crystals were not forthcoming. Although these two compounds have planar piperidine rings, **11** performs the ionic interaction with Arg60 through its "*meta*" carboxylic acid. The variation in the position
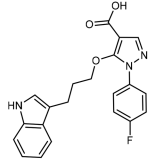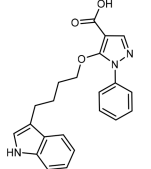
of the carboxylic acid attached to the phenyl rings causes a 3-fold difference of affinity between the two compounds.

Finally, **16** is the only compound to have a benzodioxepinyl group and an oxobutanoic acid attached to position 7 of the benzyl group. Although the restraints are caused by the fusion of the benzo and dioxepinyl rings on the flexibility of the oxobutanoic acid moiety, this fragment also interacts with the Arg60 through the carboxylic acid. However, the benzodioxepin moiety does not superpose well with the position of the other fragments with different linkers between the two rings,

and instead, only the dioxepinyl ring sits in the same binding site as the phenyl group of fragment **10**.

Applying SAR by Catalog Using Fragment 1 to Obtain New Leads with a Low-Micromolar Affinity against MtDHFR. Fragment **1** binds to the glycerol pocket of MtDHFR with a K_D of 0.640 mM (LE = 0.28) and it was selected for further elaboration and optimization. Since the aryl rings of the compound play an important role in the affinity to MtDHFR, it was decided that both rings should be maintained during any further optimization. On the basis of fragment **1**, a campaign of SAR was explored using an in-house library (Supplementary Methods). Initially, DSF was used to identify compounds that had a higher ΔT_m than fragment **1**, and several compounds were identified, and the affinities of these were assessed using ITC (Table 2 and Figure S7). These

Table 2. Calorimetric Analysis of Derivatives from Fragment 1
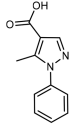
Compound	ΔTm (ºC)	Kd (μM)	LE
Frag 1	1.2	641±124	0.28
1a	3.3	192±84	0.19
1b	3.3	--	---
1c	3.6	34±8	0.22
1d	5.1	17±2	0.24
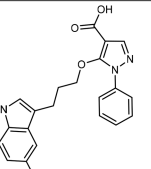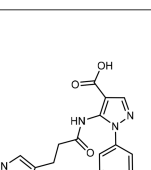
compounds have the scaffold of Fragment **1** and an indole moiety connected with different linkers (Table 2). The ITC assay indicated a significant increase of affinity for three molecules, in the range of 10, 20, and 40-fold greater than the initial fragment, while the LE decreased only slightly for the compounds **1c** and **1d**, respectively (Table 2). The best of

these compounds (**1d**) had a K_D of 17 μM and has a propylamine linker.

The complexes of MtDHFR:NADPH with these 4 compounds had their crystallographic structures solved (Figure 4 and Table S3), and the analysis indicates that the gain of the
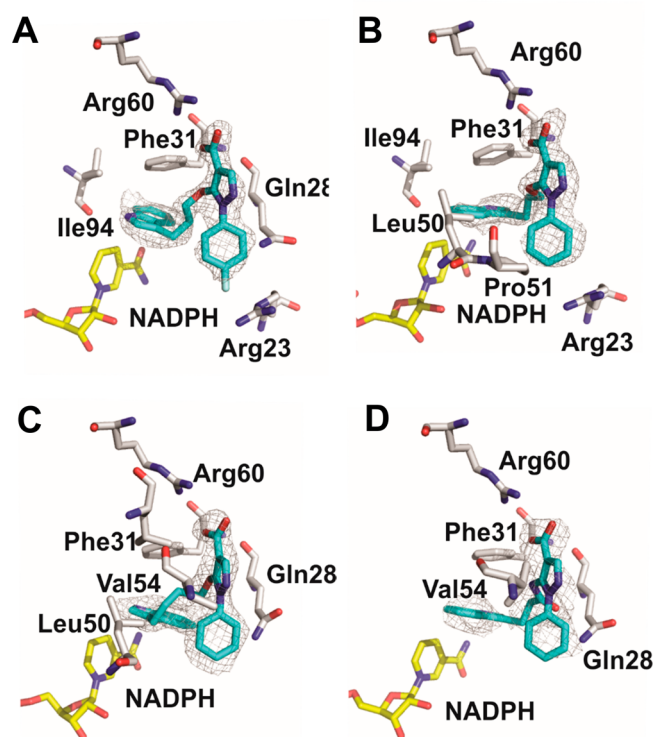
Figure 4. Crystallographic structures of MtDHFR:NADPH in complex with compounds derived from Fragment **1**. (A) **1a**; (B) **1b**; (C) **1c**; and (D) **1d**. The electron density is based on a $2F_o-F_c$ map with a 1σ contours.

affinity of **1d** could be provided by the oxygen of the propanamide group linker that forms a new hydrogen bond interaction with Gln28 side chain in contrast to the other compounds of this series (Figure 4). The analysis of the structures of the complexes indicates that probably a shorter linker is favorable to accommodating these compounds in the active site and performing π-interaction with Phe31. However, because of its flexibility, the linker can adopt different conformations as well as the indole ring, although this always performs a π interaction with a Phe31. In contrast, the fluorine atom attached to the aryl ring of the compound **1a** seems to strongly and unfavorably influence the affinity of this compound as it has the lowest affinity among these series. The addition of the methyl group on the indole ring of compound **1c** also could decrease the affinity of this compound in contrast to the **1d**. The thermodynamic analysis of **1d** indicates a high entropic penalty in comparison with the other compounds of the series (Figure S7).

However, these four compounds have lost their interaction with the glycerol-binding pocket adopting the binding mode of position 1, which is shown in Figure 3A1, most likely due to the strong interaction between the indole group and Phe31, and the favorable interaction of the carboxylic acid with the Arg60 at the active site entrance. Further optimization is

necessary to maintain chemical functional groups in this pocket.

The compounds based on fragment **1** show that the development of new DHFR inhibitors based on a pyrimidine-free scaffold is feasible, and a more stepwise approach for fragment growing, expanding into the rest of the active site while maintaining the glycerol-binding site interaction, should be possible. As the glycerol-binding site is a specific feature of MtDHFR, selective compounds targeting *M. tuberculosis* rather than hDHFR could be obtained. In future works, different organic chemistry strategies associated with computational techniques could be successfully applied to generate specific and potent pyrimidine-free compounds targeting MtDHFR.

We have successfully applied a FBDD approach to MtDHFR and have identified and confirmed the interactions of 21 molecules. This is the first report of a FBDD campaign against any DHFR, and surprisingly, many of the identified compounds have completely novel scaffolds not reported for any DHFR. Through subsequent screening of an in-house library, derivatives of one of the molecules (**1**) were identified and binding assessed, showing improved affinities from 600 μM to 17 μM, although interactions with the glycerol binding site were lost. However, the identification of these lead molecules opens possibilities in the identification of a completely novel series of compounds targeting MtDHFR and that could move forward to *in vivo* studies.

■ CONCLUSION

Dihydrofolate reductases are one of the most studied and explored enzymes in strategies of drug discovery against infectious and human diseases. However, there are no effective drugs designed specifically to target MtDHFR. We applied an integrated strategy of FBDD, which also has so far not been applied to any DHFR. Using the combination of several molecular biophysical techniques, we have identified a series of compounds with completely novel scaffolds that bind in nonexplored regions of the MtDHFR active site. These new chemical molecules open perspectives in the development of alternative molecules to treat tuberculosis. Additionally, our findings may also inspire the development of new DHFR inhibitors against other different infectious diseases.

■ METHODS

Protein Production and Preparation. MtDHFR was produced according to the protocol established by Dias et al.[28] and that of Ribeiro et al.[30] Alternatively, for crystallization experiments, the *folA* gene from *M. tuberculosis* inserted into a pET20(b) to produce a Histidine-tag free protein and expression and lysate were also prepared as reported in Ribeiro et al.[30] For purification of the Histidine-tag free MtDHFR, the supernatant was loaded onto a gravity methotrexate-agarose column (Merck), eluted using 1 mM of dihydrofolate, and dialyzed against 20 mM potassium phosphate pH 7.5 and 50 mM KCl (buffer A). For both constructs, the proteins were further purified using an S200 16/60 gel filtration chromatography column (GE Healthcare) previously equilibrated with buffer A.

Differential Scanning Fluorimetry (DSF). DSF assays were performed in a PCR iCycler (BioRad) coupled to an iQ5Multicolor Real-Time PCR Detection System (Bio-RAD). 96 well plates were used in with each well containing a total volume of 100 μL consisting of 95% (v/v) buffer A, 5% (v/v)

DMSO, 2.5× SYPRO Orange dye (Invitrogen), and 1 mM NADPH (Sigma-Aldrich). The final concentration of MtDHFR in each well was 3 μM. 80 wells of the plate were used to screen different fragments, which had a concentration of 5 mM, 8 wells were used as positive controls (5 mM of trimethoprim), and 8 wells were used only in the presence of 5% DMSO as "negative control". 1250 fragment-like compounds from the Maybridge RO3 library were tested. For the assays, the plates were heated from 25 to 75 °C at increments of 0.5 °C per minute. The fluorescence intensity of SYPRO Orange dye was monitored, with excitation−emission wavelengths of 490/575 nm, as a function of temperature. The ΔT_m was calculated from the difference of the average values of all "negative controls" (reference) and that of the protein in the presence of fragments. A positive hit was defined as a compound that increased the melting temperature by ≥0.5 °C.

STD-NMR Assays. For NMR experiments, the fragments were initially dissolved using DMSO-d_6 and further diluted using D$_2$O at a final concentration of 500 μM, and the protein in buffer A was diluted to 5 μM. The NMR spectra were obtained using an Agilent DD2 500 MHz spectrometer equipped with a triple-resonance probe at 298 K. The 1D STD-NMR spectra were obtained by the subtraction of saturated spectra (on resonance) from the reference spectra (off-resonance) after identical processing and phasing. The subtraction of on-resonance spectra from off-resonance spectra was performed automatically by phase cycling using the dpfgse_satzfer pulse sequence implemented in the VNMRJ software (Agilent). The 1D STD-NMR spectrum was acquired using 8192 scans with a selective irradiation frequency of protein at −0.5 ppm for on-resonance and at 30 ppm for off-resonance. 40 G-shaped pulses of 50 ms separated by a 1 ms of delay were applied to the protein. The total length of the saturation train was 2.04 s. A T$_2$ filter was applied to eliminating all protein background. The off-resonance spectrum was used as a reference spectrum and acquired with 4096 scans keeping all the other parameters equal to the 1D STD-NMR spectrum. For the group epitope mapping analysis, the STD enhancements were determined by the integrals of individual protons of the ligands in the 1D STD_NMR spectrum divided by the integral of the same signals at the reference spectrum.

Isothermal Titration Calorimetry (ITC). ITC assays were performed on a MicroCal VP-ITC2000 or iTC200 (Malvern). For both, cell and syringe solutions contained 95% (v/v) buffer A, 1 mM NADPH and 5% (v/v) DMSO. The cell solution contained between 30 and 50 μM of MtDHFR for experiments performed using VP-ITC2000 or between 100 to 160 μM for experiments using an iTC200. Compounds were dissolved at a concentration ranging from 2 to 10 mM in buffer A with 5% DMSO and 1 mM NADPH. The titration constituted of 20 to 25 injections using different volumes for VP-ITC2000 (first injection of 3 μL followed by 24 injections of 10 μL) and iTC200 (first injection of 0.2 μL followed by 19 injections of 2.2 μL) at 26 °C. The heats of dilutions were subtracted from the titration data prior to curve fitting. The curves were fitted by nonlinear least-squares regression using the noninteracting one-site or sequential-binding models using Origin 7.0 (Microcal).

Crystallography and Structure Analysis. The crystallization of MtDHFR was performed by the vapor diffusion method using a hanging-drop strategy using the protocol described by Ribeiro et al.[30] with modifications. Briefly, 1 μL of

Tag-free MtDHFR at 10 mg/mL, previously incubated with 10 mM of NADPH, was mixed in a coverslip with 1 μL of a crystallization condition constituted by 1.6 M ammonium sulfate, 100 mM MES (2-(*N*-morpholino)ethanesulfonic acid), pH 6.5, 10 mM CoCl$_2$ and inverted down against the 300 μL of crystallization solution added in the wells of Linbro plate (Hampton Research). Bipyramidal crystals of MtDHFR appeared after 3–4 days at 18 °C. Complexes of the holoenzyme (MtDHFR:NADPH) with fragments and compounds were obtained by cocrystallization or soaking as described in Table 1. For cocrystallization, solutions containing MtDHFR, NADPH, and 20–60 mM of different fragments were prior incubated for about 30 min on ice. For soaking experiments, about 50 to 100 mM of a compound solution was added to a drop containing crystals of holoenzyme for 10 min to 20 h, prior to crystal harvesting and freezing.

The X-ray data collection was effected at different synchrotron sources (Table S2). The data processing was performed using XDS[31] and scaled by Aimless[32] from the CCP4 suite.[33] The structures were solved by molecular replacement using Phaser MR[34] from Phenix crystallographic suite[35] and the PDB entry 1DF7[29] as a search model. The crystallographic refinement was performed using Phenix.Refine[36] followed by manual inspection using COOT.[37] The stereochemical quality of the models was checked using MolProbilty[38] and the figures were prepared using PyMol (The PyMOL Molecular Graphics System, Version 2.0 Schrödinger, LLC).

■ ASSOCIATED CONTENT

Ⓢ Supporting Information

The Supporting Information is available free of charge at https://pubs.acs.org/doi/10.1021/acsinfecdis.0c00263.

Supplementary Experimental Section; Thermal Shift (DSF) analysis of MtDHFR; Fragment-hits identified by DSF; 1D STD-NMR analysis of the positive fragments; Isotherms for ITC assays for the fragment interactions with MtDHFR; Superposition of MtDHFR:NADPH in complex with fragments; Superposition of MtDHFR-NADPH-**10** and MtDHFR-NADPH-MTX; Thermodynamic analysis of MtDHFR:NADPH with compounds; Calorimetric analysis of fragments against MtDHFR; Crystallographic data for MtDHFR in complex with fragments; Crystallographic data for MtDHFR in complex with compounds (PDF)

■ AUTHOR INFORMATION

Corresponding Author

Marcio V. B. Dias − *Department of Microbiology, Institute of Biomedical Science, University of São Paulo, São Paulo, SP 05508-000, Brazil; Institute of Biology, University of Campinas, Campinas, SP 13083-862, Brazil; Department of Biology, IBILCE-State University of São Paulo, São José do Rio Preto, SP 15054-000, Brazil; Department of Biochemistry, University of Cambridge, Cambridge CB2 1GA, U.K.; Department of Chemistry, University of Warwick, Coventry CV4 7AL, U.K.;* ⓞ orcid.org/0000-0002-5312-0191; Email: mvbdias@usp.br

Authors

João A. Ribeiro − *Department of Microbiology, Institute of Biomedical Science, University of São Paulo, São Paulo, SP 05508-000, Brazil; Institute of Biology, University of Campinas, Campinas, SP 13083-862, Brazil*

Alexander Hammer − *Department of Chemistry, University of Cambridge, Cambridge CB2 1EW, U.K.*

Gerardo A. Libreros-Zúñiga − *Department of Microbiology, Institute of Biomedical Science, University of São Paulo, São Paulo, SP 05508-000, Brazil; Department of Biology, IBILCE-State University of São Paulo, São José do Rio Preto, SP 15054-000, Brazil; Department of Microbiology, University of Valle, Cali 760043, Colombia;* ⓞ orcid.org/0000-0003-0196-1957

Sair M. Chavez-Pacheco − *Department of Microbiology, Institute of Biomedical Science, University of São Paulo, São Paulo, SP 05508-000, Brazil*

Petros Tyrakis − *Department of Biochemistry, University of Cambridge, Cambridge CB2 1GA, U.K.*

Gabriel S. de Oliveira − *Department of Microbiology, Institute of Biomedical Science, University of São Paulo, São Paulo, SP 05508-000, Brazil*

Timothy Kirkman − *Department of Chemistry, University of Warwick, Coventry CV4 7AL, U.K.*

Jamal El Bakali − *Department of Chemistry, University of Cambridge, Cambridge CB2 1EW, U.K.*

Silvana A. Rocco − *National Laboratory of Biosciences, Campinas, SP 13083-100, Brazil*

Mauricio L. Sforça − *National Laboratory of Biosciences, Campinas, SP 13083-100, Brazil*

Roberto Parise-Filho − *Department of Pharmacy, Faculty of Pharmaceutical Sciences, University of São Paulo, São Paulo, SP 05508-000, Brazil*

Anthony G. Coyne − *Department of Chemistry, University of Cambridge, Cambridge CB2 1EW, U.K.;* ⓞ orcid.org/0000-0003-0205-5630

Tom L. Blundell − *Department of Biochemistry, University of Cambridge, Cambridge CB2 1GA, U.K.*

Chris Abell − *Department of Chemistry, University of Cambridge, Cambridge CB2 1EW, U.K.;* ⓞ orcid.org/0000-0001-9174-1987

Complete contact information is available at:
https://pubs.acs.org/10.1021/acsinfecdis.0c00263

Author Contributions

MVBD, CA, AGC, and TLB designed the research; MVBD and PT performed the initial screening on DSF; JAR, GALZ, and GSO performed ITC experiments and analysis; SAR and MLS performed the STD-NMR; JAR, SMC-P, PT, and MVBD solved the structures, AH, JE-B, and AGC performed the SAR by catalog of compounds; JAR, AH, GALZ, SMC-P, TM, RPF, AGC, and MVBD analyzed and interpreted the results; MVBD compiled the results; AGC and MVBD wrote the manuscript.

Notes

The authors declare no competing financial interest.
The coordinates and structure factor files were deposited in the PDB with the following entries: 6VS5 (MtDHFR:NADPH:**Frag1**); 6VS6 (MtDHFR:NADPH:**Frag2**); 6VS8 (MtDHFR:NADPH:**Frag3**); 6VVB (MtDHFR:NADPH:**Frag10**); 6VS9 (MtDHFR:NADPH:**Frag11**); 6VSD (MtDHFR:NADPH:**Frag13**); 6VSE (MtDHFR:NADPH:**Frag14**); 6VSF (MtDHFR:NADPH:**Frag1**); 6VSF (MtDHFR:NADPH:**Frag16**); 6VSG (MtDHFR:NADPH:**Frag17**); 6VV6 (MtDHFR:NADPH:**1a**); 6VV9 (MtDHFR:NADPH:**1b**); 6VV7 (MtDHFR:NADPH:**1c**); 6VV8 (MtDHFR:NADPH:**1d**).

■ REFERENCES

(1) Dias, M. V. B., Santos, J. C., Libreros-Zúñiga, G. A., Ribeiro, J. A., and Chavez-Pacheco, S. M. (2018) Folate biosynthesis pathway: mechanisms and insights into drug design for infectious diseases. *Future Med. Chem.* 10 (8), 935−959.

(2) Gonen, N., and Assaraf, Y. G. (2012) Antifolates in cancer therapy: structure, activity and mechanisms of drug resistance. *Drug Resist. Updates* 15 (4), 183−210.

(3) Cipriani, P., Ruscitti, P., Carubbi, F., Liakouli, V., and Giacomelli, R. (2014) Methotrexate: an old new drug in autoimmune disease. *Expert Rev. Clin. Immunol.* 10 (11), 1519−1530.

(4) Morgan, A., Cofer, C., and Stevens, D. L. (2009) Iclaprim: a novel dihydrofolate reductase inhibitor for skin and soft tissue infections. *Future Microbiol.* 4 (2), 131−144.

(5) Müller, I. B., and Hyde, J. E. (2013) Folate metabolism in human malaria parasites—75 years on. *Mol. Biochem. Parasitol.* 188 (1), 63−77.

(6) Sharma, M., and Chauhan, P. M. (2012) Dihydrofolate reductase as a therapeutic target for infectious diseases: opportunities and challenges. *Future Med. Chem.* 4 (10), 1335−1365.

(7) Yang, X., Wedajo, W., Yamada, Y., Dahlroth, S.-L., Neo, J.J.-L., Dick, T., and Chui, W.-K. (2018) 1,3,5-triazaspiro[5.5]undeca-2,4-dienes as selective Mycobacterium tuberculosis dihydrofolate reductase inhibitors with potent whole cell activity. *Eur. J. Med. Chem.* 144, 262−276.

(8) Mugumbate, G., Abrahams, K. A., Cox, J. A. G., Papadatos, G., van Westen, G., Lelièvre, J., Calus, S. T., Loman, N. J., Ballell, L., Barros, D., Overington, J. P., and Besra, G. S. (2015) Mycobacterial dihydrofolate reductase inhibitors identified using chemogenomic methods and in vitro validation. *PLoS One* 10 (3), No. e0121492.

(9) Kumar, A., Zhang, M., Zhu, L., Liao, R. P., Mutai, C., Hafsat, S., Sherman, D. R., and Wang, M. W. (2012) High-throughput screening and sensitized bacteria identify an M. tuberculosis dihydrofolate reductase inhibitor with whole cell activity. *PLoS One* 7 (6), No. e39961.

(10) Hajian, B., Scocchera, E., Shoen, C., Krucinska, J., Viswanathan, K., G-Dayanandan, N., Erlandsen, H., Estrada, A., Mikušová, K., Korduláková, J., Cynamon, M., and Wright, D. (2019) Drugging the folate pathway in Mycobacterium tuberculosis: the Role of multi-targeting agents. *Cell Chem. Biol.* 26 (6), 781−791.

(11) Chakraborty, S., Gruber, T., Barry, C. E., Boshoff, H. I., and Rhee, K. Y. (2013) Para-aminosalicylic acid acts as an alternative substrate of folate metabolism in Mycobacterium tuberculosis. *Science* 339 (6115), 88−91.

(12) Zheng, J., Rubin, E. J., Bifani, P., Mathys, V., Lim, V., Au, M., Jang, J., Nam, J., Dick, T., Walker, J. R., Pethe, K., and Camacho, L. R. (2013) Para-aminosalicylic acid Is a prodrug targeting dihydrofolate reductase in Mycobacterium tuberculosis. *J. Biol. Chem.* 288 (32), 23447−23456.

(13) Dawadi, S., Kordus, S. L., Baughn, A. D., and Aldrich, C. C. (2017) Synthesis and analysis of bacterial folate metabolism intermediates and antifolates. *Org. Lett.* 19 (19), 5220−5223.

(14) Pai, M., Behr, M. A., Dowdy, D., Dheda, K., Divangahi, M., Boehme, C. C., Ginsberg, A., Swaminathan, S., Spigelman, M., Getahun, H., Menzies, D., and Raviglione, M. (2016) Tuberculosis. *Nat. Rev. Dis. Primers* 2, 16076.

(15) Barthod, L., Lopez, J.-G., Curti, C., Bornet, C., Roche, M., Montana, M., and Vanelle, P. (2018) News on therapeutic management of MDR-tuberculosis: a literature review. *J. Chemother.* 30 (1), 1−15.

(16) Erlanson, D. A., Fesik, S. W., Hubbard, R. E., Jahnke, W., and Jhoti, H. (2016) Twenty years on: the impact of fragments on drug discovery. *Nat. Rev. Drug Discovery* 15 (9), 605−619.

(17) Heikkila, T. J., Surade, S., Silvestre, H. L., Dias, M. V. B., Ciulli, A., Bromfield, K., Scott, D., Howard, N., Wen, S., Wei, A. H., Osborne, D., Abell, C., and Blundell, T. L. (2009) Fragment-Based Drug Discovery in Academia: Experiences from a Tuberculosis Programme. In *From Molecules to Medicines* (Sussman, J. L., and Spadon, P., eds.), NATO Science for Peace and Security Series A: Chemistry and Biology, Springer, Dordrecht.

(18) Mashalidis, E. H., Sledź, P., Lang, S., and Abell, C. (2013) A three-stage biophysical screening cascade for fragment-based drug discovery. *Nat. Protoc.* 8 (11), 2309−2324.

(19) Hung, A. W., Silvestre, H. L., Wen, S., Ciulli, A., Blundell, T. L., and Abell, C. (2009) Application of fragment growing and fragment linking to the discovery of inhibitors of Mycobacterium tuberculosis pantothenate synthetase. *Angew. Chem., Int. Ed.* 48 (45), 8452−8456.

(20) Silvestre, H. L., Blundell, T. L., Abell, C., and Ciulli, A. (2013) Integrated biophysical approach to fragment screening and validation for fragment-based lead discovery. *Proc. Natl. Acad. Sci. U. S. A.* 110 (32), 12984−12989.

(21) Dai, R., Geders, T. W., Liu, F., Park, S. W., Schnappinger, D., Aldrich, C. C., and Finzel, B. C. (2015) Fragment-based exploration of binding site flexibility in *Mycobacterium tuberculosis* BioA. *J. Med. Chem.* 58 (13), 5208−5217.

(22) Marchetti, C., Chan, D. S. H., Coyne, A. G., and Abell, C. (2018) Fragment-based approaches to TB drugs. *Parasitology* 145 (02), 184−195.

(23) Mendes, V., and Blundell, T. L. (2017) Targeting tuberculosis using structure-guided fragment-based drug design. *Drug Discovery Today* 22 (3), 546−554.

(24) Congreve, M., Carr, R., Murray, C., and Jhoti, H. (2003) A ″rule of three″ for fragment-based lead discovery? *Drug Discovery Today* 8 (19), 876.

(25) Srinivasan, B., Rodrigues, J. V., Tonddast-Navaei, S., Shakhnovich, E., and Skolnick, J. (2017) Rational design of novel allosteric dihydrofolate reductase inhibitors showing antibacterial effects on drug-resistant Escherichia coli escape variants. *ACS Chem. Biol.* 12 (7), 1848−1857.

(26) Mayer, M., and Meyer, B. (2001) Group epitope mapping by saturation transfer difference NMR to identify segments of a ligand in direct contact with a protein receptor. *J. Am. Chem. Soc.* 123 (25), 6108−6117.

(27) Sugiki, T., Furuita, K., Fujiwara, T., and Kojima, C. (2018) Current NMR techniques for structure-based drug discovery. *Molecules* 23 (1), 148.

(28) Dias, M. V. B., Tyrakis, P., Domingues, R. R., Paes-Leme, A. F., and Blundell, T. L. (2014) Mycobacterium tuberculosis dihydrofolate reductase reveals two conformational states and a possible low affinity mechanism to antifolate drugs. *Structure* 22 (1), 94−103.

(29) Li, R., Sirawaraporn, R., Chitnumsub, P., Sirawaraporn, W., Wooden, J., Athappilly, F., Turley, S., and Hol, W. G. (2000) Three-dimensional structure of M. tuberculosis dihydrofolate reductase reveals opportunities for the design of novel tuberculosis drugs. *J. Mol. Biol.* 295 (2), 307−323.

(30) Ribeiro, J. A., Chavez-Pacheco, S. M., Oliveira, G. S., Silva, C. S., Giudice, J. H. P., Libreros-Zúñiga, G. A., and Dias, M. V. B. (2019) Crystal structures of the closed form of Mycobacterium tuberculosis

dihydrofolate reductase in complex with dihydrofolate and antifolates. *Acta Crystallogr. D Struct. Biol.* 75 (7), 682−693.

(31) Kabsch, W. (2010) XDS. *Acta Crystallogr., Sect. D: Biol. Crystallogr.* 66 (2), 125−132.

(32) Evans, P. R., and Murshudov, G. N. (2013) How good are my data and what is the resolution? *Acta Crystallogr., Sect. D: Biol. Crystallogr.* 69 (Pt7), 1204−1214.

(33) Winn, M. D., Ballard, C. C., Cowtan, K. D., Dodson, E. J., Emsley, P., Evans, P. R., Keegan, R. M., Krissinel, E. B., Leslie, A. G., McCoy, A., McNicholas, S. J., Murshudov, G. N., Pannu, N. S., Potterton, E. A., Powell, H. R., Read, R. J., Vagin, A., and Wilson, K. S. (2011) Overview of the CCP4 suite and current developments. *Acta Crystallogr., Sect. D: Biol. Crystallogr.* 67 (Pt4), 235−242.

(34) McCoy, A. J., Grosse-Kunstleve, R. W., Adams, P. D., Winn, M. D., Storoni, L. C., and Read, R. J. (2007) Phaser crystallographic software. *J. Appl. Crystallogr.* 40 (Pt4), 658−674.

(35) Adams, P. D., Afonine, P. V., Bunkóczi, G., Chen, V. B., Echols, N., Headd, J. J., Hung, L. W., Jain, S., Kapral, G. J., Grosse-Kunstleve, R. W., McCoy, A. J., Moriarty, N. W., Oeffner, R. D., Read, R. J., Richardson, D. C., Richardson, J. S., Terwilliger, T. C., and Zwart, P. H. (2011) The phenix software for automated determination of macromolecular structures. *Methods* 55 (1), 94−106.

(36) Afonine, P. V., Grosse-Kunstleve, R. W., Echols, N., Headd, J. J., Moriarty, N. W., Mustyakimov, M., Terwilliger, T. C., Urzhumtsev, A., Zwart, P. H., and Adams, P. D. (2012) Towards automated crystallographic structure refinement with phenix.refine. *Acta Crystallogr., Sect. D: Biol. Crystallogr.* 68 (Pt4), 352−367.

(37) Emsley, P., and Cowtan, K. (2004) Coot: model-building tools for molecular graphics. *Acta Crystallogr., Sect. D: Biol. Crystallogr.* 60 (Pt12), 2126−2132.

(38) Chen, V. B., Arendall, W. B., Headd, J. J., Keedy, D. A., Immormino, R. M., Kapral, G. J., Murray, L. W., Richardson, J. S., and Richardson, D. C. (2010) MolProbity: All-atom structure validation for macromolecular crystallography. *Acta Crystallogr., Sect. D: Biol. Crystallogr.* 66 (Pt1), 12−21.